JOURNAL OF
EMERGING INVESTIGATORS

Article

Enhanced brain arteries and aneurysms analysis using a CAE-CFD approach

Vineet Saravanan[1], Selvi Saravanan[1]
[1] Cranbrook Kingswood Upper School, Bloomfield Hills, Michigan

SUMMARY

Brain aneurysms, also known as cerebral aneurysms or intracranial aneurysms, affect approximately 3.2% of the global population and are responsible for nearly 500,000 deaths annually. Remarkably, half of these fatalities occur in individuals under the age of 50, with women at higher risk than men (3:2 ratio). Neurologists, neuroradiologists, and neurosurgeons are therefore exploring ways to minimize potentially fatal outcomes. One tool used to detect these aneurysms is magnetic resonance angiography (MRA). Yet, misdiagnosis or suboptimal treatment occurs in up to one-quarter of patients upon initial medical consultation. Hence, it is essential to develop better approaches that enable doctors to detect brain aneurysms from MRA images. We propose a novel approach using a computer-aided engineering (CAE) process to analyze the aneurysm and surrounding arterial structures. In this CAE process, 2D or 3D MRA images were converted to computer-aided design (CAD) models that facilitate analysis of blood flow patterns using computational fluid dynamics (CFD). The CFD simulations computed hemodynamic parameters such as wall shear stress (WSS), velocity vectors representing blood flow direction and speed, and particle tracking to visualize blood flow patterns, which are crucial for assessing rupture risk. This innovative modeling and simulation approach improved our ability to predict aneurysm behavior, increasing risk assessment accuracy and potentially supporting better surgical planning. Our preliminary research indicates that this methodology may assist as a simulation tool to explore treatment decisions. Clinical testing may lead to advanced neurosurgical diagnostics and might eventually pave the way for more effective personalized treatment strategies for brain aneurysms.

INTRODUCTION

A brain aneurysm forms when a weakened section of a blood vessel in the brain swells and fills with blood over time (1). Primary contributing factors to arterial wall weakness leading to brain aneurysms include family history, congenital abnormalities, aging, trauma or injury, infections, health conditions like high blood pressure or vascular conditions, and lifestyle habits such as smoking or drug use (2). A specialist doctor treating brain aneurysms considers the above factors, along with aneurysm type, size, shape, and location information, to determine the best treatment option for an unruptured aneurysm (2). The Brain Aneurysm Foundation reports that approximately 1 out of 50 people have some form of an unruptured brain aneurysm, which is roughly 6.7 million individuals in the United States (3). Each year, around 30,000 individuals in the United States and 500,000 globally suffer from a ruptured brain aneurysm, with one rupture occurring every 18 minutes on average (3).

Brain aneurysms, also known as cerebral aneurysms, are classified into three types (4). The first and most prevalent type, known as a saccular or berry aneurysm, typically develops in the arteries at the base of the brain, accounts for 80% of cases, and is most frequently seen in adults (2). These aneurysms possess shape characteristics, including a neck, stem, and dome, significantly impacting hemodynamics. These structural features not only contribute to the risk of rupture but also play a critical role in determining the most appropriate treatment options. The second common type of brain aneurysm is the fusiform aneurysm, where the artery balloons along the entire perimeter, bulging out on all sides (2). These aneurysms consist of an outpouching of the arterial wall; hence, no stem exists. Fusiform aneurysms mainly occur in the middle cerebral artery (MCA) and have a higher fatality rate than saccular aneurysms, primarily because fusiform aneurysms are often larger, involve longer artery segments and are more challenging to treat (2). The third and rarest type of brain aneurysm is a mycotic aneurysm, which results from infections that weaken artery walls (3).

Brain aneurysms are categorized into three sizes based on their approximate diameters: small to medium aneurysms, which are under 11 mm (about the size of a pencil eraser); large aneurysms, ranging between 11 to 25 mm (about the size of a dime); and giant aneurysms, larger than 25 mm (about the size of a quarter) (4). Aneurysms over 3 mm typically have a higher risk of bursting and need more immediate treatment (5). To provide a perspective on these dimensions within healthy adult brain arteries: the anterior cerebral artery (ACA) at its origin measures 2.61 mm in diameter and 7.68 mm in length, the posterior cerebral artery (PCA) measures 2.70 mm in diameter and 52 mm in length, and the MCA measures 3.00 mm in diameter and 26.70 mm in length (6).

Brain aneurysms are often diagnosed using a combination of imaging scans and tests, including computed tomography scan/angiography (CT scan/CTA), magnetic resonance imaging/angiogram (MRI/MRA), cerebral angiography, and cerebrospinal fluid (CSF) analysis by performing a spinal tap (2). An MRA is an MRI scan focusing specifically on blood vessels. Overall, MRA is the most popular of all the methods as it is non-invasive, does not require inserting a catheter into the body, doesn't expose patients to ionizing radiation, and uses a magnetic field and radio wave pulses to create images (7). In addition to being noninvasive, MRA is reliable in detecting brain aneurysms larger than 3 mm in

https://doi.org/10.59720/24-156

size and can provide detailed information with good spatial resolution (8). Some limitations of MRA imaging are magnetic field inhomogeneities, structural complexities, and partial visualization. Inexperienced operators may also misinterpret normal anatomical variations or artifacts as aneurysms, and the inability to see calcification or thrombosis can lead to underestimation of the aneurysm's complexity (7-9). The three most common methods of MRA analysis are time-of-flight, phase-contrast, and contrast-enhanced MRA, commonly referred to in the medical industry as TOF-MRA, PC-MRA, and CE-MRA. TOF-MRA is the most prevalent due to its ability to capture small vessels without contrast agents and its high spatial resolution (7).

Using MRA data, a computer-aided detection system has been explored to aid in detecting common types of brain aneurysms (9,10). However, some of these approaches were primarily focused on detecting brain aneurysms based on the shape and size of aneurysms only (10). In our study, we went deeper by evaluating hemodynamic factors such as wall shear stress (WSS), velocity vectors, and particle tracking with complete patient data. These aspects are critical because they provide insights into how blood flow, velocity, and pressure interact with vessel walls and aneurysm structures. These factors can be obtained by applying computational fluid dynamics (CFD), which is traditionally used in fluid engineering (11,12). Hence, to better understand aneurysm growth and rupture risk, we integrated this advanced computational technique, CFD, into the MRA analysis process, allowing us to assess hemodynamic parameters. This CFD improvement could be a tool to enhance clinical decisions on aneurysm assessments and risk stratification, and further extending this with simulations may allow for better treatment planning.

In this study, we hypothesized that in a berry aneurysm, the blood flow may increase localized stress on the dome, raising the risk of rupture, similar to a meandering river where water flow erodes the outer curve. We also related brain aneurysms to an inflated balloon with a constant flow of air: as blood continuously flows, the pressure builds inside the aneurysm, and the wall stretches and thins with time, increasing the risk of rupture. We aimed to quantify hemodynamic parameters across aneurysms to understand their potential impact on the risk of aneurysm rupture.

Our objective was to utilize a CFD analysis of the aneurysm and surrounding artery region to extract hemodynamic data useful for patient diagnosis. Our research methodology began with pre-processed 2D or 3D MRA images, which we used to build a model of isolated brain arteries and then performed CFD analysis (**Figure 1**). The CFD analysis provided WSS evaluation, velocity vector fields, and particle flow tracking behavior of each aneurysm. Our study's combination of 3D visualization and CFD analysis could give a quantitative approach to understanding aneurysms, providing additional insights for neuroradiology practices and clinical management of brain aneurysms.

RESULTS

Our work in this paper used the TOF-MRA open dataset comprising 284 subjects, including 157 patients with 198 aneurysms (13). The creation of the artery reconstructions from the MRA images involved the removal of the skull from these images and the application of field correction techniques to enhance image quality. We randomly went through data sets of 75 patients with aneurysms, and the slices of 2D MRA images were converted to 3D models using the 3D Slicer App. Then, we went through 3D computer-aided design (CAD) visualization by reviewing seventy-five models and picked three models for further study. A model with a fusiform aneurysm, a model with a berry aneurysm, and a model with a complex aneurysm. All models had one blood inlet with multiple outlets for blood flow focusing on the aneurysm zone. These three models, taken from the open data set mentioned before, had patient-specific geometries, including shapes of blood vessels with aneurysms, to proceed with our steps of the computer-aided engineering (CAE) process (**Figure 1**). For the CAE process, the segmented images were refined during the CAD processing stage to reduce image complexity and repair imperfections. Then, the surface and solid models were converted into a mesh format suitable for CFD simulation. We used this mesh and physics information in CFD analysis to simulate and analyze the hemodynamics within the arteries and determine blood flow, velocity, and pressure and their impact on the arterial walls.

The first hemodynamics factor, WSS, quantifies the tangential force per unit area applied by blood flow on the inner walls of the blood vessels. This parameter is critical for understanding the mechanical forces contributing to brain aneurysms. A low WSS can lead to wall weakening and aneurysm formation, while a high WSS may increase stress on the arterial wall, contributing to aneurysm rupture (14). The second hemodynamics factor, velocity vector, represents the direction and magnitude of blood flow within the vessel or aneurysm. Analyzing velocity vectors helps identify flow patterns, such as swirling or stagnation zones within an aneurysm, linked to wall weakening. High velocity can increase the stress on the wall, especially in narrow or turbulent regions. The third hemodynamics factor, particle tracking, is a technique to visualize the trajectories of particles in the blood flow, mimicking the motion of blood cells. The

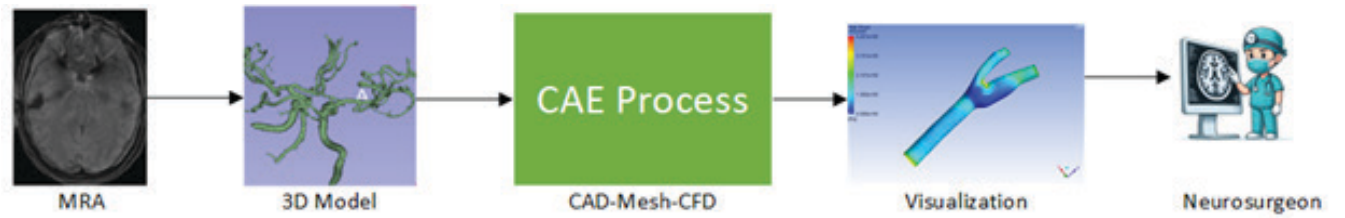

Figure 1: Overview of research workflow. The initial 2D MRA image series was converted to 3D through a tool. CAD processing refines the 3D image into a cleaner mesh that is acceptable for CFD software to solve. CFD analysis was performed using all the physics and boundary conditions provided (see Methods). The CFD image is then visualized in a 3D viewer with rotation and zoom functionality so the neurosurgeon can interpret the image.

https://doi.org/10.59720/24-156

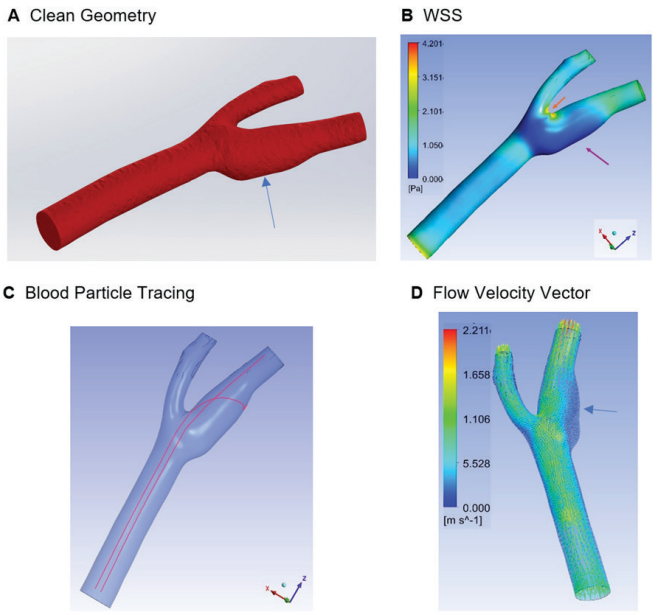

Figure 2: Model of a fusiform aneurysm. (A) From the MRA image, the model was cleaned as part of CAD pre-processing, a step before meshing. The blue upward-pointing arrow reflects the precise physical geometry of the aneurysm. (B) WSS was higher, as indicated by an orange downward-pointing arrow, at the bifurcation area and lower at the aneurysm, as indicated by a purple upward-pointing arrow. (C) A simulation of two blood particles taken around the center of the inlet showed that one particle impacted the bifurcation region and further impacted the aneurysm area, while the other exited through the right outlet. (D) Blood flow had a higher velocity away at the center of artery walls and a lower velocity in the aneurysm zone.

direction of blood flow impacts the distribution of stress on the aneurysm. When blood flow hits the aneurysm at certain angles, it can create high-pressure areas, further weakening the wall.

Our first CAD model was of a patient with a fusiform aneurysm (**Figure 2a**). The fusiform aneurysm model had an inlet diameter of 3.15 mm with artery bifurcation into two varying outlet sizes of 2.25 mm and 1.50 mm. The fusiform aneurysm was on the outlet with a 2.25 mm diameter. We observed heightened WSS with a value of 4.2 Pa at the bifurcation (**Figure 2b**). This was much higher than the healthy WSS range of 0.5 to 2.0 Pa (14). The WSS was higher near the bifurcation point than the fusiform aneurysm on the right-side artery. The right-side outlet, where the fusiform aneurysm was located, had lower WSS due to the diversion of blood flow from one smaller inlet along the Z-direction into two more prominent outlets along the X-Y plane. Similarly, we noted elevated WSS at the transition from the artery to the aneurysm, with high WSS at the aneurysm neck. We simulated the fusiform aneurysm with two massless blood particles for particle tracking around the center of the inlet, where the blood fluid velocity was highest at 115 cm/s. The path line of particle tracking provides a detailed view of flow trajectories, showing how blood enters, circulates, and exits aneurysms or vessels. The simulation of two path lines began near the center of the inlet, where blood velocity was highest. One path line impacted the arterial bifurcation, while the other struck near the start of the fusiform aneurysm, creating high-velocity impact points. (**Figure 2c**). Furthermore, the velocity vectors for the fusiform aneurysm showed that the blood fluid velocity was about 100 cm/s near the bifurcation (**Figure 2d**). The normal range for middle cerebral artery blood velocity should be between 30 to 100 cm/s (15). Thus, the blood fluid velocity of approximately 100 cm/s indicates that this patient needs preventive measures or treatment.

The second model was for a patient with a berry aneurysm. This is the most common type of brain aneurysm and can occur at the junction of the ACA with PCA or the PCA with MCA (13). This model had a saccular aneurysm measuring 6.10 mm in one outlet. We selected this model for two reasons: a prior study showed that the mean size of ruptured aneurysms was 6.10 mm, and this type of aneurysm with sizes larger than 5 mm should be treated (16, 17). Our model found a WSS of 5.0 Pa at the bifurcation and 2.6 Pa at the base of the berry aneurysm (**Figure 3a**). The average WSS for large arteries typically falls around 1 to 2.5 Pa, which is considered optimal for maintaining vascular health; however, in this model, the WSS values exceeded 2.5 Pa. (15). Simulations of two massless blood particles from the center of the inlet showed impacts at the bifurcation and base of the aneurysm (**Figure 3b**). The velocity flow vector slowed inside the balloon and increased to 251 cm/s right after that area (**Figure 3c**). These simulations revealed that the blood impacted the edge of the vessel at the onset of the aneurysm, highlighting a high-risk zone that may require intervention. This supported our hypothesis of higher stress near the aneurysm opening and lower stress inside the aneurysm.

The third model was a patient with complex aneurysms at multiple locations of varying sizes (**Figure 4**). These aneurysms were a partial mix of fusiform and berry types. This model had an inlet of 2.70 mm in diameter, with a first split into two outlets and a final total of four outlets of varying sizes. The first outlet at the bottom left had a 1.97 mm diameter, with its branch outlet having a diameter of 1.52 mm. The second outlet has a 1.73mm diameter, with its branch outlet of 0.86mm at top left. The smaller aneurysm of 2.95 mm was at the bifurcation point towards first outlet. The bigger aneurysm of 4.65 mm was at the bifurcation point towards second outlet. The aneurysm measuring 4.65 mm had a WSS of 1.5 Pa and velocity vectors of 237 cm/s. For bigger aneurysm, compared to the normal range, WSS values were at the higher end for WSS and over the healthy limit for the velocity vector, indicating a higher risk and need for treatment (15). The two outlets were influenced by the varying sizes, shapes, and pressures of the arteries, which extended from the inlet to the four outlets. (**Figure 4**). For these complex or mixed aneurysms, the WSS provided better support for diagnosis through this additional visualization (**Figure 4a**). Overall, the CFD analysis offered better visualization capabilities compared to traditional 2D or 3D artery geometry visualizations based on MRI data.

DISCUSSION

MRA is a standard tool used to detect brain aneurysms. The current approach with MRA is to have the visual interpretations by neuroradiologists provided by 2D imaging or processed into a 3D model. However, some limitations may impact its accuracy and diagnostic utility, including variations in magnetic field, which affects image quality and may cause operators to misinterpret anatomical variations

https://doi.org/10.59720/24-156

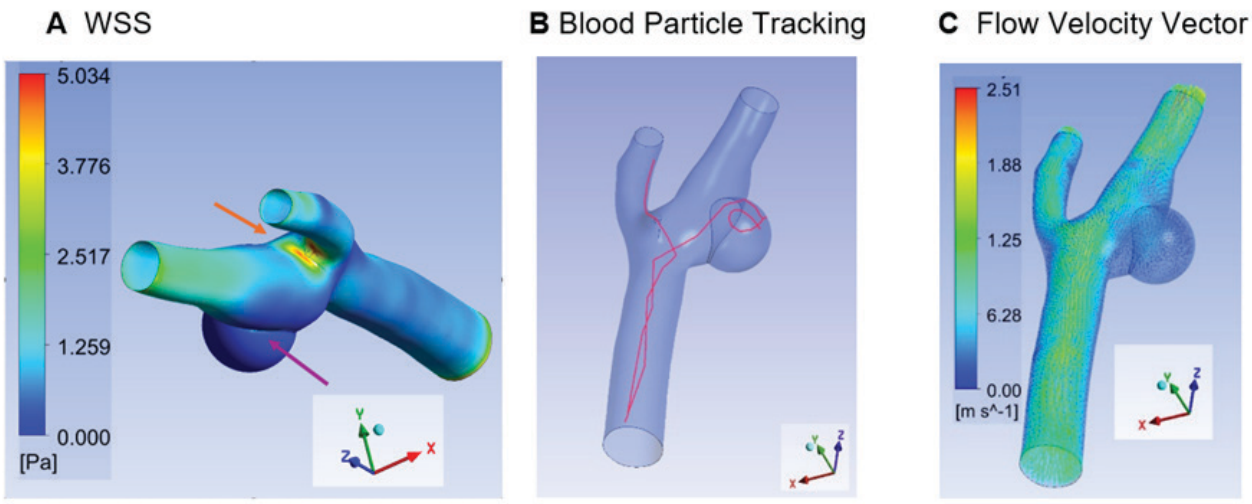

Figure 3: Model of a berry aneurysm. (A) WSS depicts the highest stress in bifurcation, as indicated by the orange downward pointing arrow, and higher at the aneurysm neck, as indicated by the purple upward pointing arrow. (B) Two blood particles were taken at the center of the inlet. One impacting the bifurcation and another impacting the aneurysm neck. (C) Blood had a higher velocity at the center of the artery. Lower velocity both near the artery walls and inside the aneurysm.

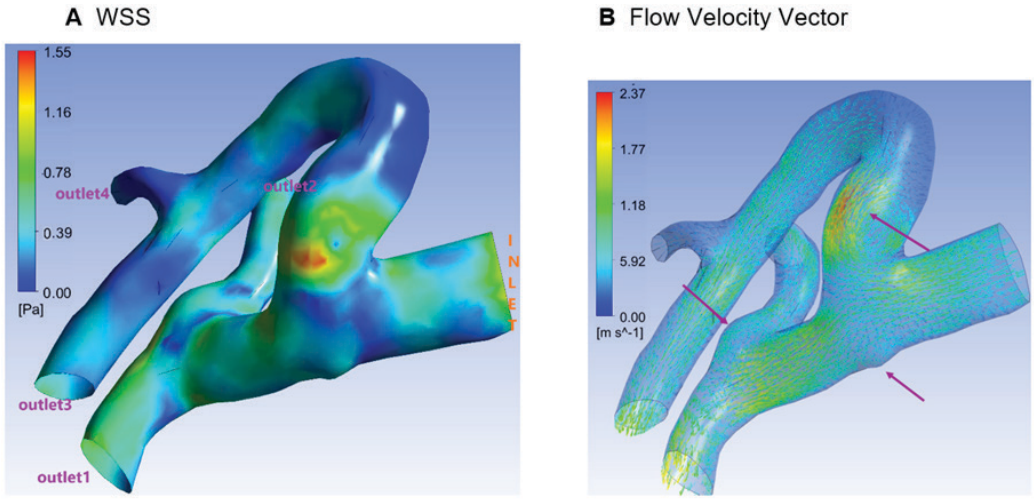

Figure 4: Model of a complex aneurysm. Blood enters through an inlet from the right and undergoes a first split through a larger artery followed by a further split into two more outlets. (A) WSS was highest, as seen in red, on the aneurysm due to its shape and size. (B) Three aneurysms of varying sizes were marked with purple arrows. Blood velocity was highest in the zone, as seen in red, marked up top upward pointing purple arrow. This could be due to an irregularly shaped region.

or imaging artifacts, leading to false positives or negatives. To improve reliability, we proposed a novel approach to use MRA data and incorporate a CAE process to analyze aneurysms and surrounding arterial structures. As part of CAE, patient-specific geometry in the TOF-MRA open data set was used in our CAD-CFD approach (**Figure 5**). Hence, our approach considers the four significant factors currently used in predicting an aneurysm rupture: the aneurysm's shape, size, thickness of the blood vessel wall, and location (5). To investigate the value of this approach, models of three different kinds of aneurysms were used: a fusiform aneurysm, a berry aneurysm, and a complex aneurysm. This way, the major types of brain aneurysms were analyzed. After fluid flow analysis, the visualization of the results offered an enhanced visual representation of hemodynamic factors (WSS, velocity vector, and particle tracking), helping to improve the understanding of how they interact and contribute to the overall impact of the aneurysm. Our engineering approach to medicine can be considered as a potential tool to minimize misdiagnosis, as we are using image processing and obtaining a more visual representation of the impact of the aneurysm (18, 19).

From our work, we observed that WSS was higher at the neck of the berry aneurysm and was lower inside the dome of the aneurysm. High-gradient WSS or rapid changes in WSS near the dome of an aneurysm indicate a higher risk of rupture (14). Regions of low WSS cause degradation of the arterial wall, contributing to aneurysm bursts, which aligns with our hypothesis that an inflated balloon with constant airflow leads to a burst (14). Our three models' WSS results show peaks

https://doi.org/10.59720/24-156

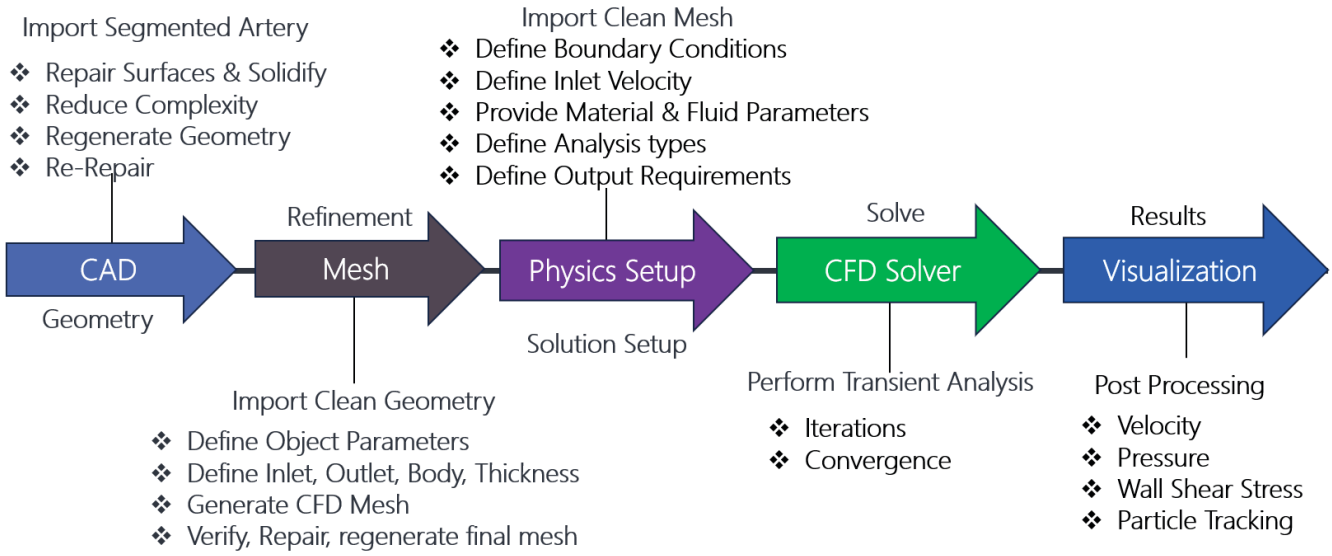

Figure 5: CAE Process. For our work, we performed five distinct steps. The first step was CAD, where we imported a segmented artery with an aneurysm. Geometry clean-up was performed to create a smooth, continuous model suitable for meshing and repairing inconsistencies such as gaps, overlapping surfaces, and invalid edges. The second step was meshing, which involved dividing a geometry into smaller discrete elements to facilitate accurate numerical simulations, with finer meshes generally improving precision by better capturing the geometry's details and flow characteristics. The third step was setting up physics and boundary conditions, which involved defining the physical properties and behaviors, fluid dynamics, and inlet/outlet conditions for simulation. The fourth step was performing transient analysis with a CFD solver to calculate the fluid flow behavior over time, capturing the dynamic changes in pressure, velocity, and flow rate at each time step to simulate time-dependent processes. In the fifth step, the output data from the solver, which was a large volume of data at each node and element, was processed through a 3D result visualization tool, as post-processing was essential for viewing in graphical form.

at the bifurcation of the artery and at the neck of the berry aneurysm. This was in line with a simplified study done in the past that reported maximum WSS was at the neck of berry aneurysm (45%) and at the artery bifurcation (40%), with the remaining WSS at various spots based on specific anatomical features of the patient (20).

Based on our observations in this study, which were related to velocity vectors, we saw higher velocities at bifurcations and aneurysm necks. The velocity was very low inside the dome of the berry aneurysm and the swollen portion of the fusiform aneurysm. This is consistent with our hypothesis that the river velocity is high when the main flow of water encounters an obstacle or changes direction, creating a localized area of rotating water and lower velocity in the bay, providing a slow or resting spot. When blood flow changes abruptly, such as at bifurcation points or aneurysm necks, it exerts a force on the wall, which experiences an equal opposing force, leading to higher stress and aneurysm formation at these critical points. These results support the fundamental physics principle that fluid shear stress is directly related to the velocity gradient orthogonal to the flow direction.

Our work, which utilized the TOF-MRA open dataset, did not include actual blood pressure data. Arteries experience diastolic pressure for a longer duration than systolic pressure. For a healthy individual, the mean arterial pressure can be calculated as diastolic + (systolic – diastolic)/3 which gives a value of 93.33 mmHg (21). In individuals at risk for aneurysms, blood pressure is often elevated above this value and can fluctuate over time. Therefore, a static blood pressure value of 100 mm Hg was used in our study (22). In clinical practice, this model can and should be adjusted on a case-by-case basis to reflect the specific blood pressure of individual patients.

In our study, the direction of blood inflow with particle tracking through high-velocity blood cells from the center of the inlet indicates the collision mostly with the neck of the aneurysm and at the bifurcation point. These trajectories create collisions, causing damage to the material on the artery wall at the bifurcation and neck of the aneurysm. By simulating particle trajectories, clinicians can predict how blood flow will behave after interventions like coiling or stent placement.

Complex flow patterns, characterized by varying flow rates and velocities, were better understood by using CFD, which maps how velocity and particle movement affect wall shear stress. The velocity vector illustrates the impact of variations in arterial size and shape complexity on blood velocity within the vascular system. Additional benefits of CFD were the ability to factor in flow velocity variations due to relative vessel sizes, location of aneurysms relative to one another, aspect ratio (height of aneurysm/neck width), size ratio (maximum height of aneurysm/neck width), dome to neck ratio (dome diameter/neck diameter) and volume to surface area ratio (volume of aneurysm/surface area of aneurysm).

The workflow in our research, which transitions from MRA imaging to 3D CAD and subsequently to CFD analysis, allowed us to understand internal blood flow dynamics and aneurysm risk assessment. This integrated approach may be beneficial as an additional tool alongside traditional medical imaging. As a continuation of this study, additional patient models should be developed to further validate the proposed approach. Future work may even build an artificial intelligence (AI) model based on our approach to more quickly diagnose

https://doi.org/10.59720/24-156

aneurysms. Furthermore, in the future, clinical trials using this approach may pave the way for it to become a standard tool for physicians. In clinical practice, detailed models may be invaluable when evaluating treatment options like coil embolization, a procedure where the aneurysmal sac is filled with metal coils, to assess the efficacy of different coil types or sizes (21). Similarly, the suitability of various stents or the application of biocompatible glue-tissue patches on weak arterial spots can be explored. CAD and CFD simulations allow for visualizing the effects of these interventions on blood flow, offering clinicians and patients a clearer perspective on potential outcomes.

MATERIALS AND METHODS

Hardware, Software and Data Set

A standalone desktop with 32GB RAM using an Intel i7-8700 CPU running on Windows 10 Pro with 1TB solid state drive was used for all simulations. We used an Intel UHD Graphics 630 display adaptor and an NVIDIA GeForce GTX 1060 6GB graphics card. We selected datasets from 75 patients with aneurysms at random from a TOF-MRA open-source dataset comprising 284 subjects (13). The 3D Slicer app, a free and open-source platform for analyzing and understanding medical image data, was used to convert the MRA scans into 3D models (23). The models were then imported into Autodesk Fusion 360-2023 free version to convert into CAD models (24). These were then imported into Ansys Workbench 2023 R2 Student Version to perform the rest of the work, as multiple modules exist for different functionality (25). The CAD cleanup, meshing, setup, Fluent as a CFD solver, and result visualization tool were all done using this Ansys software.

Workflow

The workflow began with importing the refined MRA model and creating a cleaner CAD model (**Figure 1**). Then, the mesh was refined, physics was applied, fluid flow analysis was conducted, and the results were visualized (**Figure 5**). Each step of the workflow is described in detail below.

CAD Geometry and Mesh

3D Slicer processes MRA data into detailed 3D models of brain arteries and aneurysms. It allows users to visualize, segment, and analyze these anatomical structures in 3D, which can aid in measuring aneurysm size. We used the thresholding function with a varying threshold parameter. We started at the 0.50 threshold and then experimented to find the highest value that maximized the number of arteries selected. We then manually highlighted any remaining artery structure that was missing and removed any non-artery structure selected. 3D Slicer exported the geometry information in STL format, which was then imported into the Ansys SpaceClaim CAD software, and the segmented artery around the brain aneurysm area was trimmed and retained (**Figure 6**).

In Ansys SpaceClaim CAD software, various diagnostic moduli were employed to identify and resolve gaps, invalid faces, free and invalid edges, open surfaces, sharp curvatures, or unusual surface variations. Here, curvatures were evaluated, and all faulty faces, knitting and patching gaps, and surfaces were fixed and healed. The diagnostic tool was then rerun to address all discontinuities and problem areas (**Figure 7**). We proceeded with mesh generation once the CAD geometry had been confirmed to be topologically valid.

Mesh generation discretized the model geometry, allowing numerical computations to solve a physics problem. In finite element modeling, a mesh is a network of nodes connected by elements, where nodes represent discrete points in the geometry, and elements define the relationships between these points, enabling complex physical simulations. Small angles, very short edges, collapsing close points, and low aspect ratios were avoided when generating the triangular

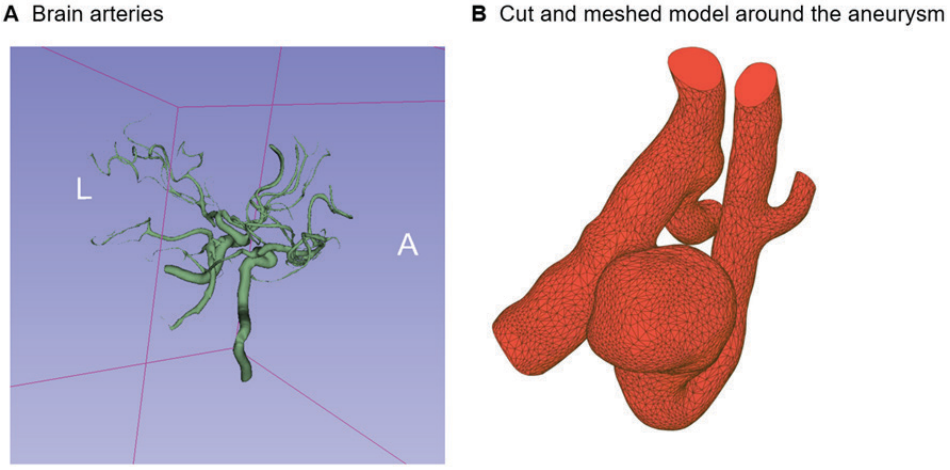

Figure 6: Arteries and aneurysm. (A) The reconstructed 3D model was visualized from the processed MRA data through the 3D slicer. As seen in the image, this step preserves all the brain's main arteries. A refers to "anterior," indicating the front part of the brain. L refers to "left," indicating the left side of the brain. (B) Once the location of the aneurysm was identified, we retained enough surrounding arteries to assess flow dynamics and structural relationships, mainly focusing on key branches or bifurcations that could impact aneurysm growth or rupture risk. That section was kept, and the rest of the areas were removed. This zone was then cleaned, refined, and meshed as a preparatory step before the CFD analysis.

https://doi.org/10.59720/24-156

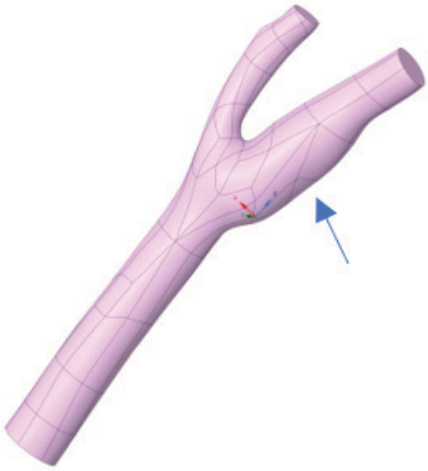

Figure 7: Model of a fusiform aneurysm, after Geometry Cleanup. The arrow points to the aneurysm after all geometric surface cleaning were completed. Geometry cleanup involved repairing gaps, invalid edges, and overlapping surfaces to ensure the model was free of defects. This step was crucial for creating a clean, continuous geometry that was ready for meshing and accurate simulations, preventing errors during downstream analysis.

mesh through iterative refinement, where the mesh was continuously evaluated and adjusted. Special attention was given to areas near the aneurysm neck and dome to ensure a precise representation of critical regions affecting hemodynamic analysis. The mesh flow must be smooth, meaning that the transition in average mesh size from one region to another should be gradual, not abrupt. Generally, a finer mesh, meaning higher mesh density, leads to more accurate results. However, beyond specific mesh sizes, increases in accuracy tend to diminish.

With our iterations, setting the maximum mesh size to at least a quarter of the artery wall thickness yielded optimal results. Our strategy involved using a much finer mesh around the brain aneurysm area while maintaining regular mesh in other regions, using software settings. For the first model with a fusiform aneurysm, a total of 27,337 nodes and 83,310 elements were used. For the second model with the berry aneurysm, a total of 47,534 nodes and 140,017 elements were used (**Figure 8a**). For the third model with the complex aneurysm, a total of 27,656 nodes and 70,965 elements were used (**Figure 8b**). Once the meshing was complete, the inlet, outlet, and outer surface areas for the subsequent physics setup were defined. The CFD simulation's necessary physics and boundary conditions were set up with clean geometry and refined mesh, through verification and tools provided in software (**Figure 5**).

Physics and Solution Setup

Once the mesh was cleaned, the material and fluid parameters were defined. The more common materials like air and water are Newtonian fluids. Here, the viscosity remains constant regardless of how much force is applied. However, blood similar to honey or toothpaste, are non-Newtonian fluids. Non-Newtonian fluids have a viscosity that changes with shear rate or stress or when force is applied. Traditionally, for simplicity, blood has been modeled as a Newtonian fluid, even though it is a shear-thinning non-Newtonian fluid (15). Our study employed a non-Newtonian fluid formulation to more accurately represent blood behavior.

While the patient's exact blood density can be inputted, this study used an average density of 1060 kg/m³ for all analyses. Whole blood is a liquid tissue comprising 45% cells and 55% fluid plasma. Blood cells include three components, namely, red blood cells, white blood cells, and platelets. Blood plasma is 92% water, with the remaining 8% consisting of proteins, metabolites, and ions. For our study, a blood density of 1060 kg/m³ was used, with a combination of the density of plasma (1025 kg/m³) and the density of blood cells (1125 kg/m³) (26).

Blood flow is pulsatile and cyclic. Hence, a realistic time-

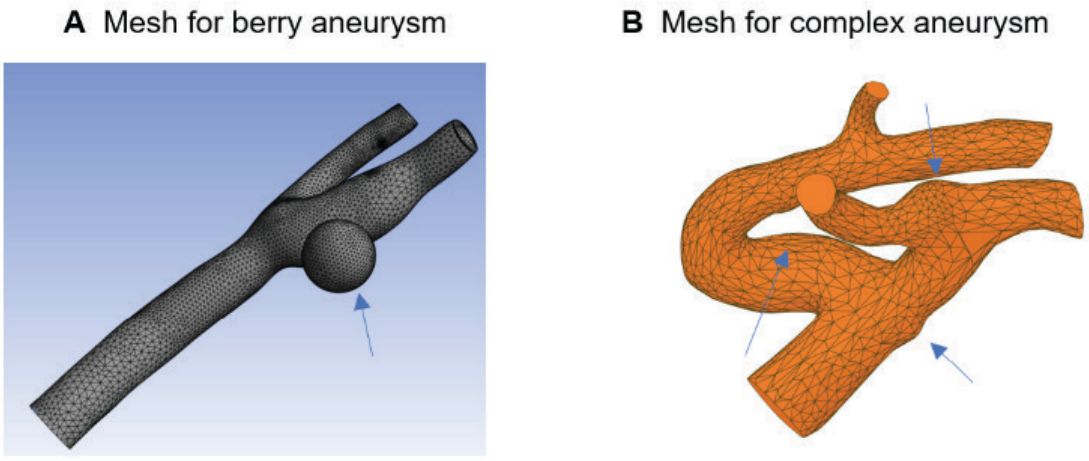

Figure 8: Model of a berry aneurysm and complex aneurysm after Meshing. The arrows point to aneurysms. Here, the mesh was not uniform throughout. (A) The mesh for the berry aneurysm had a higher density around the bifurcation and aneurysm, while a lower-density mesh was applied near the inlet and outlet. (B) The mesh for complex aneurysms had a slightly lower density at the inlet and outlets, while the remaining areas featured a higher mesh density. Due to the model's complexity, some mesh polygons were larger to maintain continuity and flow, which was acceptable for the CFD analysis.

https://doi.org/10.59720/24-156

varying velocity profile at the inlet was used to mimic the pulsatile nature of the blood flow model (22, 27). This study used time-varying blood pressure for the inlet, using a user-defined function feature in the software. The function was a sine wave for the systolic phase with a peak velocity of 0.5 m/s, a minimum velocity of 0.1 m/s, and the duration of each period of 0.8 s (22). For this analysis, the pressure at the outlet was defined to be constant at 100 mm Hg (28). The pressure comes from the average healthy human systolic pressure of 120 mm Hg and diastolic pressure of 80 mm Hg (21).

CFD Methods and Solver

The Navier-Stokes equation (NSE) forms the basis for nearly all CFD problems. Among multiple approaches to solving the NSE, the finite volume method was chosen, as it allows for using completely arbitrary grids, making it highly suitable for analyzing flows that interact with complex geometries, such as arteries and brain aneurysms. Hence, Ansys-Fluent software that solves CFD using the FVM method was employed for this research (25).

For viscosity, a few non-Newtonian mathematical fluid models were investigated for blood rheology in constricted arteries. Our work employed the Carreau fluid model for viscosity, as researchers claim Carreau's mathematical fluid model was close to experimental outcomes and truthfully forecasts the characteristics of the nature of blood in small arteries (29, 30). Once this setup process was complete, the transient analysis was performed. As no direct analytical solutions exist to solve NSE in their most general form, an iterative approach was employed to establish convergence. The three critical parameters used in our study for simulating fluid behavior over time were a time step size of 0.01 s, which is the small interval of time over which the fluid motion was calculated in each iteration; 50 time steps, which is the total number of time intervals used to simulate the flow rate over the desired solution; and a maximum iterations per time step of 100, which is the maximum iterations the solver will perform within a single time step to ensure that the solution converges before moving to the next step. A convergence criterion in CFD is based on the residuals, which measure how much the solution changes between iterations within each time step. For our solution to converge, these residuals should fall below a predefined threshold of 0.001. The physical quantities of pressure, velocity, and flow rate were monitored, and they stabilized over time to indicate convergence.

Results Visualization

The output from the CFD solver is a large data set of numerical values. For visualization purposes, the Ansys software was employed to review the results obtained from the CFD solver (25). We investigated WSS, particle tracking to study a fluid particle from inlet to outlet, and velocity in the x-, y-, and z-directions to represent the magnitude of blood flow.

Received: April 28, 2024
Accepted: September 11, 2024
Published: March 2, 2025

REFERENCES

1. "Brain Aneurysm. Symptoms and Causes." *Mayo Clinic, Mayo Foundation for Medical Education and Research.* www.mayoclinic.org/diseases-conditions/brain-aneurysm/symptoms-causes/syc-20361483002E. Accessed 01 Oct. 2023.
2. "Cerebral Aneurysms." *National Institute of Neurological Disorders and Stroke.* www.ninds.nih.gov/health-information/disorders/cerebral-aneurysms. Accessed 22 Oct. 2023.
3. "Statistics and Facts." *Brain Aneurysm Foundation.* www.bafound.org/statistics-and-facts/. Accessed 01 Sep. 2023.
4. "What Is a Brain Aneurysm?" *WebMD.* www.webmd.com/brain/brain-aneurysm. Accessed 06 Dec. 2023.
5. "Four Aneurysm Traits that Predict Rupture." *Johns Hopkins Medicine.* www.hopkinsmedicine.org/health/conditions-and-diseases/4-aneurysm-traits-that-predict-rupture. Accessed 10 Dec. 2023.
6. Hassan N. H., *et al.* "Anatomical Measurements of Cerebral Arteries Using Digital Subtraction Angiography." *AIN Shams Medical Journal,* vol. 71, no. 2, Jun. 2020, pp. 259-267. https://doi.org/10.21608/asmj.2020.125617.
7. Lotfi H-B. and James M. P. "Current Imaging Assessment and Treatment of Intracranial Aneurysms." A*merican Journal of Roentgenology,* vol. 196, no. 1, Jan. 2011, pp. 32-44. https://doi.org/10.2214/AJR.10.5329.
8. "Brain (Cerebral) Aneurysm Imaging" *Medscape by WebMD LLC, Global resource for health care professionals.* emedicine.medscape.com/article/337027-overview. Accessed 12 Nov. 2023.
9. Štepán-Buksakowska I. L., *et al.* "Computer-aided diagnosis improves detection of small intracranial aneurysms on MRA in a clinical setting." *American Journal of Neuroradiology,* vol. 35, no. 10, Oct. 2014. https://doi.org/10.3174/ajnr.A3996.
10. Hayashi H., *et al.* "Development of Cerebral Aneurysm Computer-Aided Detection Systems With 3D MRA Data." *Yokogawa Corporation of America,* no. 39, 2005. www.yokogawa.com/us/library/resources/yokogawa-technical-reports/development-of-cerebral-aneurysm-computer-aided-detection-systems-with-3d-mra-data/. Accessed 12 Aug. 2024.
11. Rahma A. G., Yousef K., and Abdelhamid T. "Blood Flow CFD Simulation on a Cerebral Artery of a Stroke Patient." *SN Applied Sciences,* vol. 4, no. 261, 7 Sep. 2022. https://doi.org/10.1007/s42452-022-05149-y.
12. Muhsin K., Saleh G., and Jorg S. "An analytical method informed by clinical imaging data for estimating outlet boundary conditions in computational fluid dynamics analysis of carotid artery blood flow." *Scientific Reports* 13, article no. 14973, 11 Sep. 2023. https://doi.org/10.1038/s41598-023-42004-5.
13. Di Noto T., *et al.* "Towards Automated Brain Aneurysm Detection in TOF-MRA: Open Data, Weak Labels, and Anatomical Knowledge." *Neuroinformatics,* vol. 21, no. 1, Jan. 2023, pp. 21-34. https://doi.org/10.1007/s12021-022-09597-0.
14. Mutlu O., *et al.* "How Does Hemodynamics Affect Rupture Tissue Mechanics in Abdominal Aortic Aneurysm: Focus on Wall Shear Stress Derived Parameters, Time-Averaged Wall Shear Stress, Oscillatory Shear Index, Endothelial Cell Activation Potential, and Relative Residence Time." *Computers in Biology and Medicine,* vol. 154, Jan. 2023. https://doi.org/10.1016/j.compbiomed.2023.106609.
15. Liu H., *et al.* "Comparison of Newtonian and Non-

https://doi.org/10.59720/24-156

Newtonian Fluid Models in Blood Flow Simulation in Patients With Intracranial Arterial Stenosis." *Frontiers in Physiology,* vol. 12. Sep. 2021. https://doi.org/10.3389/fphys.2021.718540.
16. Sanchez S., *et al.* "Morphological Characteristics of Ruptured Brain Aneurysms: A Systematic Literature Review and Meta-Analysis." *Stroke: Vascular and Interventional Neurology,* vol. 3, no. 2, Jan. 2023, https://doi.org/10.1161/SVIN.122.000707.
17. "Cerebral Aneurysm. Symptoms, Diagnosis and Treatments." *American Association of Neurological Surgeons.* aans.org/en/Patients/Neurosurgical-Conditions-and-Treatments/Cerebral-Aneurysm. Accessed 14 Sep. 2023.
18. Mayer P. L., et al. "Misdiagnosis of Symptomatic Cerebral Aneurysm: Prevalence and Correlation With Outcome at Four Institutions." *Stroke- American Heart Association,* vol. 27, no. 9, Sep. 1996, pp. 1558-1564. https://doi.org/10.1161/01.STR.27.9.1558.
19. Jou L. D. and Mawad M. E., "Analysis of Intra-Aneurysmal Flow for Cerebral Aneurysms with Cerebral Angiography." *American Journal of Neuroradiology,* vol. 33, no. 9, Oct. 2012, pp. 1679-1684. https://doi.org/10.3174/ajnr.A3057.
20. Adib M. and Hisham M. A. "Measurement of Threshold Image Intensities on Difference of Vascular Model: Effect on Computational Fluid Dynamics for Patient-Specific Cerebral Aneurysm." *Journal of Biomimetics, Biomaterials and Biomedical Engineering,* vol. 27, May 2016, pp. 55–59. https://doi.org/10.4028/www.scientific.net/JBBBE.27.55.
21. Marsh L. M. M. *Computational Fluid Dynamics of Intracranial Aneurysms: Eulerian and Lagrangian Analysis of the Effect of Endovascular Treatment on Hemodynamics.* 14 Aug. 2023. University of Washington, PhD dissertation. hdl.handle.net/1773/50492. Accessed 01 Mar. 2024.
22. Sinnott M., Cleary P. W., and Prakash M. "An Investigation of Pulsatile Blood Flow in a Bifurcation Artery Using a Grid-Free Method." *ResearchGate,* 15 Dec. 2006, researchgate.net/publication/238589397_An_investigation_of_pulsatile_blood_flow_in_a_bifurcation_artery_using_a_grid-free_method. Accessed 19 Sep. 2023.
23. Fedorov A., *et al.* "3D Slicer as an image computing platform for the Quantitative Imaging Network." *Elsevier Magnetic Resonance Imaging,* vol. 30, no. 9, Nov. 2012, pp. 1323-1341. https://doi.org/10.1016/j.mri.2012.05.001.
24. Autodesk. "Fusion 360 for Education." *Autodesk Education.* autodesk.com/education/edu-software/fusion. Accessed 10 Nov 2023.
25. ANSYS Inc. "ANSYS Student Software." *ANSYS.* ansys.com/academic/students/ansys-student. Accessed 20 Nov 2023.
26. Elert G., "Density of Blood. The Physics Factbook." *An encyclopedia of scientific essays.* hypertextbook.com/facts/2004/MichaelShmukler.shtml. Accessed 18 Nov. 2023.
27. Marmarelis V. Z., *et al.* "Time-Varying Modeling of Cerebral Hemodynamics." *IEEE Transactions on Bio-Medical Engineering,* vol. 61, no. 3, Mar. 2014, pp. 694-704. https://doi.org/10.1109/TBME.2013.2287120.
28. Beard D. A., *et al.* "A Computational Analysis of the Long-Term Regulation of Arterial Pressure." *F1000Research,* vol. 2, no. 208, 6 Dec. 2013. https://doi.org/10.12688/f1000research.2-208.v2.
29. Wajihah S. A. and Sankar D. S. "A Review on Non-Newtonian Fluid Models for Multi-Layered Blood Rheology in Constricted Arteries." *Archive of Applied Mechanics,* vol. 93, no. 5, 31 Jan. 2023, pp. 1771–1796, https://doi.org/10.1007/s00419-023-02368-6.
30. Akbar N. S. and Nadeem S. "Carreau Fluid Model for Blood Flow Through a Tapered Artery with a Stenosis." AIN Shams Engineering Journal, vol. 5, no. 4, Dec. 2014, pp. 1307–1316, https://doi.org/10.1016/j.asej.2014.05.010.